

Accepted Manuscript

Variation of radiative forcings and global warming potentials from regional aviation NO_x emissions

Agnieszka Skowron, David S. Lee, Ruben R. De León



PII: S1352-2310(14)00991-1

DOI: [10.1016/j.atmosenv.2014.12.043](https://doi.org/10.1016/j.atmosenv.2014.12.043)

Reference: AEA 13493

To appear in: *Atmospheric Environment*

Received Date: 9 August 2014

Revised Date: 12 December 2014

Accepted Date: 17 December 2014

Please cite this article as: Skowron, A., Lee, D.S., De León, R.R., Variation of radiative forcings and global warming potentials from regional aviation NO_x emissions, *Atmospheric Environment* (2015), doi: 10.1016/j.atmosenv.2014.12.043.

This is a PDF file of an unedited manuscript that has been accepted for publication. As a service to our customers we are providing this early version of the manuscript. The manuscript will undergo copyediting, typesetting, and review of the resulting proof before it is published in its final form. Please note that during the production process errors may be discovered which could affect the content, and all legal disclaimers that apply to the journal pertain.

Variation of radiative forcings and global warming potentials from regional aviation NO_x emissions

Agnieszka Skowron^{*}, David S. Lee and Ruben R. De León

Dalton Research Institute, Manchester Metropolitan University, John Dalton Building, Chester Street,
Manchester M1 5GD, United Kingdom.

^{*}Corresponding author. E-mail: a.skowron@mmu.ac.uk, tel: + 44 (0) 161 247 6703 (A. Skowron).

Abstract: The response to hemispherical and regional aircraft NO_x emissions is explored by using two climate metrics: radiative forcing (RF) and Global Warming Potential (GWP). The global chemistry transport model, MOZART-3 CTM, is applied in this study for a series of incremental aircraft NO_x emission integrations to different regions. It was found that the sensitivity of chemical responses per unit emission rate from regional aircraft NO_x emissions varies with size of aircraft NO_x emission rate and that climate metric values decrease with increasing aircraft NO_x emission rates, except for Southeast Asia. Previous work has recognized that aircraft NO_x GWPs may vary regionally. However, the way in which these regional GWPs are calculated are critical. Previous studies have added a fixed amount of NO_x to different regions. This approach can heavily bias the results of a regional GWP because of the well-established sensitivity of O₃ production to background NO_x whereby the Ozone Production Efficiency (OPE) is greater at small background NO_x. Thus, even a small addition of NO_x in a clean-air area can produce a large O₃ response. Using this ‘fixed addition’ method of 0.035 Tg(N) yr⁻¹, results in the greatest effect observed for North Atlantic and Brazil, ~10.0 mW m⁻²/Tg(N)yr⁻¹. An alternative ‘proportional approach’ is also taken that preserves the subtle balance of local NO_x-O₃-CH₄ systems with the existing emission patterns of aircraft and background NO_x, whereby a proportional amount of aircraft NO_x, 5% (N) yr⁻¹, is added to each region in order to determine the response. This results in the greatest effect observed for North Pacific that with its net NO_x RF of 23.7 mW m⁻²/Tg(N)yr⁻¹ is in contrast with the ‘fixed addition’ method. For determining regional NO_x GWPs, it is argued that the ‘proportional’ approach gives more representative results. However, a constraint of both approaches is that the regional GWP determined is dependent on the relative global emission pattern, so if that changes in the future, the regional NO_x GWP will change.

Keywords: Aviation, regional emissions, nitrogen oxides, GWP, non-linearities

1 Introduction

36
37
38
39 Aviation NO_x emissions result in a short-term increase in tropospheric ozone (O₃) and the
40 long-term destruction of a fraction of the ambient methane (CH₄), with positive and negative
41 radiative forcing responses, respectively. In addition, the CH₄ reduction results in a long-term
42 reduction in tropospheric O₃ and a long-term reduction in stratospheric water vapour from
43 reduced oxidation of CH₄, both negative radiative forcing effects. The aircraft net NO_x
44 response (the sum of all these components) is thought to result in a positive (warming)
45 radiative forcing (RF) under constant emissions assumptions (e.g., Lee et al., 2010)

46
47 The geographical imbalance of climate impact from NO_x emissions is a result of both the
48 short-term nature of the chemistry and the heterogeneous pattern of emissions; as well as, it
49 arises from complexity of the response of NO_x effect components. The short-lived O₃ change
50 (positive climate forcing, warming) is inhomogeneous, concentrated mainly where the NO_x
51 emissions occur. The CH₄ response (negative climate forcing, cooling), due to its decadal
52 lifetime, is homogeneously spread over the globe. Thus, even if these two effects might cancel
53 as a global mean, they do not on a regional scale (e.g., Prather et al., 1999).

54
55 The same amount of NO_x emissions might lead to different regional climate impacts. The O₃
56 production formed from NO_x emissions strongly depends on the background conditions that
57 are distinct for specific spatio-temporal locations. The O₃ response is influenced by the
58 background NO_x concentrations (e.g., Isaksen et al., 1978, Berntsen and Isaksen, 1999), the
59 abundance of HO_x, VOCs (e.g., Lin et al., 1988, Jaeglé et al., 1998) or the intensity of solar
60 flux. These different influences result in quite a specific behaviour, as different climate
61 responses might result from equal global mean RFs arising from the same amount of emitted
62 NO_x at different locations (e.g., Berntsen et al., 2005, Shine et al., 2005).

63
64 In this study we explore the global responses from regional emissions, by employing the
65 'popular' metrics: radiative forcing (RF) and Global Warming Potential (GWP), that have
66 been successfully exploited in other regional studies (e.g., Berntsen et al., 2005, Fry et al.,
67 2013). However, in order to explore the different aspects of regional and sub-global patterns
68 of responses, the new concepts have been also developed, e.g., the non-linear damage function

69 (Shine et al., 2005, Lund et al., 2012) or Absolute Regional Temperature Potential (Shindell,
70 2012, Collins et al., 2013).

71
72 There are only few studies dealing with geographical effects from aircraft NO_x emissions
73 (Grewe and Stenke, 2008, Stevenson and Derwent, 2009, Köhler et al., 2013). Grewe and
74 Stenke (2008) and Köhler et al. (2013) have shown that different latitudinal bands give
75 different RFs per unit aircraft NO_x emission; the RFs resultant from O₃ and CH₄ changes at
76 low latitudes are significantly greater than RFs from those changes at higher latitudes. Köhler
77 et al. (2013) also presented the aircraft NO_x impact over four geographical regions, where
78 tropical locations, China and India, with their net NO_x RFs of 14.3 mW m⁻² per Tg(N) yr⁻¹ and
79 12.6 mW m⁻² per Tg(N) yr⁻¹, substantially exceed the northern mid-latitudinal net NO_x RFs, of
80 ~2 mW m⁻² per Tg(N) yr⁻¹, over Europe and USA. On the contrary, the study of Stevenson and
81 Derwent (2009) results in strong compensations between O₃ and CH₄ responses for July's
82 pulse aircraft NO_x emissions at 112 different cruise altitude locations, where, in most cases,
83 the short-term O₃ positive RFs was overwhelmed by the long-term CH₄ negative RFs. In order
84 to illustrate the dependence of the aviation NO_x effect on the location of emission, the
85 regionally fixed amount of aircraft NO_x was applied in both, Stevenson and Derwent (2009)
86 and Köhler et al. (2013), studies.

87
88 Taking into account that the future growth of air traffic is predicted to be inhomogeneous,
89 where Asia with its developing economies is leading the way (ACI, 2011), it is important to
90 understand the spatial aviation climate responses. In this study, the atmospheric impact of a
91 series of regional aircraft NO_x emission rates is investigated using a global chemistry transport
92 model, MOZART-3 CTM. The responses from Northern and Southern Hemisphere along with
93 eight regions: Europe, North America, Southeast Asia, North Pacific, North Atlantic, Brazil,
94 South Africa and Australia are explored. This study will show that the net NO_x effect, and the
95 associated ozone and methane responses, depend not only on the location of emission, but also
96 that they vary under different experimental approaches.

97

98

99

100

101

102

103 2 Methodology

104

105 2.1 Chemistry transport model

106

107 The Model for Ozone and Related Tracers, version 3 (MOZART-3) was applied for this study.

108 This is a 3D Chemistry Transport Model (CTM) designed to simulate atmospheric ozone and

109 its precursors. It was evaluated by Kinnison et al. (2007) and used for various application

110 studies, e.g., Sassi et al. (2004), Liu et al. (2009), Wuebbles et al. (2011). Recently,

111 MOZART-3 was exploited in studies dealing with an impact of aircraft NO_x emissions on

112 atmospheric composition, e.g., Skowron et al. (2013), Søvde et al. (2014).

113

114 MOZART-3 accounts for advection based on the flux-form semi-Lagrangian scheme of Lin

115 and Rood (1996), shallow and mid-level convection (Hack, 1994), deep convective routine of

116 Zhang and MacFarlane (1995), boundary layer exchanges (Holstag and Boville 1993), or wet

117 and dry deposition (Brausser et al. (1998) and Müller (1992), respectively). MOZART-3

118 reproduces detailed chemical and physical processes from the troposphere through the

119 stratosphere, including gas-phase, photolytic and heterogeneous reactions. The kinetic and

120 photochemical data are based on the NASA/JPL evaluation (Sander et al., 2006).

121

122 The anthropogenic and biomass burning emissions are taken from Lamarque et al. (2010) and

123 represent year 2000, while the biogenic emissions are from POET (Granier et al., 2005).

124 Aircraft emissions are represented by the REACT4C base case inventory (e.g., Søvde et al.,

125 2014) for the year 2006 (CAEP/8 movements). The horizontal resolution is T42 (~ 2.8° x

126 2.8°) and the vertical domain spans 60 hybrid layers between the surface and 0.1 hPa. The

127 meteorological fields are from European Centre for Medium Range Weather Forecast

128 (ECMWF), reanalysis ERA-Interim data for the years 2004–2006 (Dee et al., 2011).

129

130 2.2 Incremental regional aircraft NO_x emissions

131

132 In order to explore the impact of regional aircraft NO_x emissions on climate, ten geographical

133 domains were defined: Europe (EUR), North America (NA), Southeast Asia (SE ASIA),

134 North Pacific (NPAC), North Atlantic (NATL), Brazil (BR), South Africa (SAFR), Australia

135 (AU), Northern Hemisphere (NH) and Southern Hemisphere (SH) (Figures 1 and 2). The

136 aircraft NO_x emissions are characterized by a heterogeneous pattern, where more than 50% of

137 aircraft NO_x emissions is present over North America, Europe and Southeast Asia. The
138 selected geographical domains constitute 62% (based on REACT4C 2006 inventory) of global
139 total aircraft NO_x emissions. Each region represents different chemical and meteorological
140 background conditions that will influence the aircraft NO_x perturbation.

141
142 Incremental aircraft NO_x emissions constitute a series of aircraft NO_x emission rates that were
143 applied to one region per experiment (Table 1). The injections of aircraft NO_x emissions are
144 valid for all altitudes in the defined domains. Each incremental aircraft NO_x case is based on
145 either an equal mass or a relative mass of emissions. The equal mass of emissions constitutes
146 different relative addition of emission to the total NO_x in each region, e.g., the injection of
147 0.035 Tg(N) yr⁻¹ is equal to ~30% increase of aircraft NO_x for northern continental regions
148 and it rises to ~160% or ~400% for oceanic or southern continental domains, respectively
149 (Table 1). The relative mass of emissions result in different amount of emitted NO_x in each
150 region. The 5% NO_x increase per year is smaller than addition of 0.035 Tg(N) yr⁻¹ by ~80–
151 95% for most of the regions. The 100% NO_x increase per year is greater than addition of 0.035
152 Tg(N) yr⁻¹ by ~70% for continental regions, but it is still smaller by ~40% for oceanic regions.

153
154 These two experimental designs address different natures of investigations. The question
155 addressed with ‘fixed NO_x’ experiments is the regional sensitivity to unit mass of emission.
156 The employment of relative aircraft NO_x emissions might be more realistic in terms of
157 defining the actual aviation NO_x effects or the assessment of the future air traffic growth.
158 Anyway, both types of experiments give useful insight into regional NO_x–O₃–CH₄ systems.

159
160 Forty six experiments were performed, one reference (base aircraft emission) run and forty
161 five perturbations (incremental aircraft emission) simulations, each starting in January 2006
162 and finishing in December 2006; each simulation was preceded by a two-year spin-up, 2004–
163 2005. The aircraft perturbation is derived by extracting the difference between ‘aircraft’ and
164 ‘incremental aircraft’ experiments. Since our experiments are performed for 3 years, the
165 magnitude of aircraft stratospheric O₃ response is not fully represented. Thus, the O₃ column
166 change presented in this paper is overestimated by 1.1%; however, the resultant O₃ RF is not
167 affected.

168

169

170

171 2.3 Metrics calculations

172
173 The monthly O₃ MOZART-3 outputs are used for short-term O₃ radiative forcing (RF)
174 calculations, using an off-line Edwards – Slingo radiation code (Edwards and Slingo, 1996).
175 The model calculates the radiative fluxes and heating rates based on the δ -Eddington form of the
176 two-stream equations in both, the long-wave and short-wave spectral regions. Cloud treatment is
177 set up based on averaged ISCCP D2 data (Rossow and Schiffer, 1999), which are used to
178 determine the position and amount of ice clouds and water in the atmosphere. Climatological
179 fields of temperature and specific humidity are determined by ERA-Interim data (Dee et al.,
180 2011).

181
182 The CH₄ concentrations change is assumed to be in equilibrium with the OH change due to
183 the aircraft NO_x perturbation from constant emissions (Fuglestedt et al., 1999). These steady-
184 state CH₄ aircraft responses are further used for long-term CH₄ RF calculations, using the
185 simplified expression defined in Myhre et al. (1998). The additional long-term effects,
186 consequently also assumed as steady-state changes, CH₄-induced O₃ and CH₄ impact on
187 stratospheric water vapour (SWV) are also calculated and defined as 50% of CH₄ RF (Myhre
188 et al., 2013) and 15% of CH₄ RF (Myhre et al., 2007), respectively.

189
190 The calculations of Global Warming Potentials (GWP) are based on a methodology described
191 by Fuglestedt et al., (2010). Assuming, that the constant one-year emission is a step emission
192 and the successive decay occurs of the resulting steady-state forcing (ΔF^{SS}) from the end of
193 the year, the AGWP can be calculated through: $AGWP(H) = \Delta F^{SS} (1 - \alpha(\exp(-H/\alpha) - \exp(-H/\alpha)))$, where H is the time horizon and α is lifetime (primary-mode lifetime in case of
194 CH₄-induced O₃ and CH₄). The CO₂ AGWPs are taken from Joos et al. (2013).

196
197

198 **3 Effects of hemispherical and regional aircraft NO_x emissions**

199

200 3.1 Chemical perturbation

201

202 The peak of O₃ perturbation is concentrated at cruise altitudes in all regions (Figure 3);
203 however, the same amount of additional aircraft NO_x (0.035 Tg(N) yr⁻¹) emitted from various
204 locations leads to different magnitudes and extents of O₃ perturbation. The NH's O₃

205 perturbation is concentrated mainly at cruise altitudes, where most of the emissions occur,
206 whilst the SH's O₃ response is observed throughout the vertical domain. This might be
207 explained by the fact by that SH's aircraft NO_x emissions are concentrated mostly in the low-
208 latitudes (there are hardly any SH's emissions for latitudes greater than 52°S), where the
209 convective transport is strong. This is the case also for BR and AU, where the chemical
210 impact has a greater vertical extent than for other regions.

211
212 The aircraft NO_x perturbation in different regions shows disparities in their impact on global
213 O₃ burden and CH₄ lifetime change (Table 2). The Southern Hemisphere produces 40% more
214 O₃ per emitted aircraft N, and is twice as efficient in CH₄ lifetime reduction, than the Northern
215 Hemisphere. A similar pattern in O₃ change is observed if the North Pacific is compared with
216 Europe. In general, the efficiency of ozone production for remote northern oceanic regions is
217 greater than for northern continental regions by 34% and this results in the larger O₃ burden
218 change for NPAC and NATL compared with EUR and NA. Among continental regions,
219 southern AU gives the greatest mass of perturbed O₃. The largest O₃ change did not always
220 introduce the greatest CH₄ reduction. The CH₄ lifetime reduction over NPAC is almost as high
221 as over SE ASIA, however NPAC's CH₄ follows the high O₃ burden change, which is not
222 observed for SE ASIA's O₃ burden change. The least efficient CH₄ loss occurs over NATL,
223 the greatest efficiency in CH₄ lifetime reduction is observed over southern BR, SAFR and AU.

224

225 3.2 Radiative forcings and global warming potentials

226

227

228 The latitudinal distributions of short-term O₃ RF for different geographical regions are shown
229 in Figure 4. In general, these patterns of RFs are governed by latitudinal profiles of regional
230 aircraft NO_x emissions. However, the magnitudes of O₃ RF responses differ: the SH's O₃ RF
231 is much larger, by 52%, than NH's short-term forcing and NPAC, NATL exceed, by 29%, the
232 O₃ responses from northern continental regions. The greatest magnitudes of short-term O₃ RF
233 responses are those from southern low-latitudes: BR, SAFR and AU, that is in contrast to their
234 aircraft NO_x emissions magnitudes.

235 Figure 5 shows the normalized net global annual mean RF and the four component forcings,
236 for different geographical regions. The inter-hemispheric differences in the resultant effects
237 are significant: both short-term O₃ RF and long-term negative RFs are twice as strong over SH
238 than over NH. The greatest net NO_x RF value is observed over North Atlantic and Brazil,

239 which is the result of strong positive short-term O₃ RF and relatively weak long-term negative
240 forcings for NATL and very strong positive short-term O₃ RF for BR. The largest short-term
241 O₃ RF and long-term CH₄ RF among northern regions is found for NPAC and SE ASIA,
242 respectively, whilst among southern regions for AU. The negative forcings play a relatively
243 large role at low-latitudes, where an efficient CH₄ oxidation leads to substantial reduction of
244 the net NO_x RF for BR, SAFR and AU, but also SE ASIA. The smallest net value of positive
245 and negative forcings is observed for North America and Europe.

246 While RF indicates the climate effects between past and present point in time, GWP gives the
247 perspective for future impact of current emissions. The aircraft NO_x GWPs from regional
248 emissions differ greatly; however, the net NO_x GWP values are positive for all regions and
249 each time horizon (Table 3). There are substantial differences in calculated GWPs; the
250 greatest values are calculated for a 20-year time horizon for each region and the significant, by
251 ~80%, reduction of GWPs appears with larger time horizons. The largest GWP values are
252 calculated for Brazil; however, for greater time horizons the North Atlantic's GWPs are
253 equally high, that is caused by less pronounced long-term negative RF effects. The smallest
254 GWP values are found for Europe for each time horizon.

255

256 3.3 Discussion

257 The differences in magnitudes of O₃ perturbation originate from various background
258 conditions specific for each region. The spatial variation of O₃ burden change has a strong
259 correlation with NO_x background concentration at flight level (Figure 6), which was also
260 presented by Stevenson and Derwent (2009), but for O₃ integrated RFs. Generally, the largest
261 global and annual O₃ burden change is observed for locations where NO_x background is low
262 and it is decreasing with greater NO_x concentrations. The SE ASIA, with large NO_x
263 background, is an exception here, as the efficiency of O₃ production charged by the intensity
264 of solar flux results in relatively large O₃ burden change.

265

266 The large O₃ response over remote oceanic regions might be unravelled by small background
267 NO_x concentrations (Figure 6). The large O₃ response over SE ASIA might be additionally
268 explained by the intensity of solar irradiance that drives the photochemistry: taking into
269 account the high NO_x background conditions in this region, the magnitude of O₃ change is

270 substantial. The mean concentration of NO_x at 227 hPa is 93 pptv, as modelled by MOZART-
271 3; however, mean local annual NO_x concentrations reach ~ 400 pptv for SE ASIA, while these
272 over mid-latitudinal regions are ~ 70 pptv. One of the factors that significantly modify SE
273 ASIA's NO_x background at flight level is the NO_x source from lightning. The SE ASIA region
274 is a receptor of 30% of global total lightning NO_x emissions at cruise altitudes; in comparison
275 to 8% for BR and less than 1% for the rest of the regions, SE ASIA's lightning NO_x is
276 significant. The southern BR, SAFR and AU O_3 responses are driven by both relatively low
277 NO_x background and solar intensity. Not only NO_x background alone, but also the relationship
278 between abundances of NO_x and photochemically generated hydrogen oxide radicals (HO_x)
279 influence the amount of O_3 that can be formed. The shift in the HO_x balance towards OH,
280 having at the same time relatively higher NO_x levels compared to HO_2 , that is the case for
281 EUR (Figure 6), increases the importance of OH+ NO_2 termination reaction chain that in turn
282 decreases the O_3 production.

283
284 The concentrations of CH_4 differ between regions within 1% range, also CO is relatively
285 uniformly distributed among investigated regions (Figure 6); both CO and CH_4 are an
286 important O_3 precursors. The CH_4 perturbations depend highly on the place and extent
287 (latitude and altitude) of the O_3 perturbation (Köhler et al., 2008), as both temperature and
288 concentrations of OH and CH_4 affect the efficiency of CH_4 oxidation. The most efficient CH_4
289 lifetime reduction occurs over SE ASIA and southern regions, BR, SAFR, AU, where
290 temperature and oxidizing conditions are the most favourable among the investigated
291 domains; the least pronounced CH_4 response is observed for NATL, that is not the case for
292 another oceanic region, NPAC. The OH and CH_4 backgrounds are of similar magnitudes over
293 NPAC and NATL; however, the temperature pattern shows differences, being higher over
294 North Pacific, by $\sim 6^\circ\text{K}$ ($\sim 3\%$) and the lower temperature slows down the CH_4 oxidation.
295 Moreover, the cruise altitudes for NATL are at 10.98 km that is one level higher than for
296 NPAC (Figure 2); aircraft NO_x emissions emitted at higher altitudes result in reduced potential
297 in CH_4 change (e.g., Skowron et al., 2013). These might be the one of the reasons of the less
298 efficient CH_4 lifetime reduction over North Atlantic.

299
300 Recently Köhler et al. (2013) presented results for regional aircraft NO_x impacts from four
301 regions: USA, Europe, India and China. The $0.036 \text{ Tg(N) yr}^{-1}$ of aircraft NO_x was injected
302 through all vertical layers into limited domains. In their study the greatest O_3 mass change and
303 O_3 forcings, as well as net NO_x forcings were found for low latitudinal regions compared with

304 northern continental regions and the net NO_x RFs and GWPs are positive. This is in agreement
305 with results from this study. However, some discrepancies appear when magnitudes of
306 responses are compared. The “continental mid-latitudinal” O_3 RFs are smaller in this study by
307 15–26% than Köhler’s et al. (2013); however, the net NO_x RFs are reported to be greater for
308 this work, by 6% for EUR and 38% for NA. It is difficult to compare the results for “northern
309 low-latitudinal” regions, as the geographical extents of investigated domains differ: in this
310 study it reaches the 12°S circle of latitude, in Köhler’s et al. (2013) – 6°N . Moreover, SE
311 ASIA region in this study is characterized by very high NO_x background concentrations from
312 lightning emissions, while Köhler’s India and China are relatively ‘free’ from those high NO_x
313 lightning emission, as modelled by MOZART-3. These might be one of the reasons of the
314 substantial differences in O_3 response and the resultant NO_x RFs over Asia.

315
316 Whilst there is a general qualitative agreement in general properties of regional responses
317 between Köhler et al. (2013) and this study, the comparison with Stevenson and Derwent
318 (2009) becomes more complicated. Their study presents integrated radiative forcings (IRF)
319 over 100-year time horizon of positive and negative responses of chemical system due to
320 aircraft NO_x emissions. The aircraft NO_x increase ($4 \text{ kg}(\text{NO}_2) \text{ s}^{-1} = 0.04 \text{ Tg}(\text{N}) \text{ yr}^{-1}$) was
321 injected for a period of month (July) at cruise altitudes ($\sim 200\text{--}300 \text{ hPa}$) in a limited
322 geographical domains. Unfortunately, a detailed comparison is not possible as Stevenson and
323 Derwent (2009) did not provide an exact number for their AGWPs. However, some
324 peculiarities are noticed, e.g., the net IRFs are negative for most of the locations. The inter-
325 model differences might play a role here; however, other aspects exist as well. Firstly, the
326 aircraft NO_x increase was performed only for a period of one month, July. The small Asian
327 short-term O_3 response may indicate that it can influence the results to some extent (the NO_x
328 background (due to lightning) is greater in this region during summer compared with winter
329 months, when the lightning NO_x ‘moves’ more south from the equator). The response of a
330 $\text{NO}_x\text{--O}_3\text{--CH}_4$ system is highly dependent on the state of the atmosphere into which aircraft
331 NO_x is injected (e.g., Stevenson et al., 2004) and a single month perturbation is not
332 representative and comparable with annual integrations when the regional responses are
333 investigated. Secondly, the amount of emitted NO_x during one month is the same as the
334 amount of NO_x applied in this study and by Köhler et al. (2013), but for a period of year. As it
335 is shown in the forthcoming Section 4, the size of NO_x emission rates influence the response
336 of the chemical system due to regional emissions.

337

338 **4 Response of the NO_x-O₃-CH₄ system for different rates of regional** 339 **aircraft NO_x emissions**

340
341 The responses of the chemical system from regional aircraft NO_x perturbations vary with the
342 size of the NO_x emissions rate and in a non-linear way (Figure 7); the greater NO_x emission
343 rates lead to weaker O₃ responses and less pronounced CH₄ reductions. However, each region
344 has its own distinctive sensitivity in the response of chemical system. The O₃ response over
345 Southeast Asia is much less sensitive to different aircraft NO_x emission rates than over oceans,
346 where the O₃ change depends significantly on the amount of emitted NO_x. For example, as a
347 result of 6.39 Tg(N) yr⁻¹ experiments, SE ASIA has the greatest global O₃ burden change and
348 NATL's O₃ is observed to be of similar magnitude as O₃ for EUR, which is in contrast to what
349 was presented in the section above. The CH₄ lifetime reduction also changes with aircraft NO_x
350 emission rates. The non-linearity of CH₄ lifetime reduction is stronger at low latitudes, where
351 conditions for CH₄ oxidation (high temperature and concentrations of OH) are advantageous,
352 compared with mid-latitudes. Thus, CH₄ over SH, SE ASIA, BR, SAFR and AU follows
353 strictly the O₃ sensitivity to additional NO_x emissions: the rate of the compensation between
354 O₃ and CH₄ remains almost the same for each incremental aircraft NO_x case (Figure 8). The
355 ratio of the CH₄ lifetime change per unit of O₃ change for SH, SE ASIA, BR, SAFR and AU
356 changes by no more than 2%, with greater NO_x emission rates. This is not observed for other
357 regions, especially oceanic domains, where CH₄/O₃ ratio becomes significantly greater (44%
358 for NATL) with larger NO_x emission rates. These results show that the variation in
359 experimental design strongly influences the magnitude of the contribution from individual
360 regions to overall chemical perturbation, e.g., the greatest O₃ burden change, can easily belong
361 to either NPAC, or SE ASIA depending on the size of aircraft NO_x emission rates.

362 363 364 **5 Variation of the effects of hemispherical and regional aircraft NO_x** 365 **emissions**

366
367 The varying regional chemical responses depend on the size of the aircraft NO_x emissions
368 (Figure 7), being especially pronounced for remote domains. The regional O₃ and CH₄
369 responses saturate with greater aircraft NO_x emission rates, where scale of this processes reach
370 different limits for each region. Equal mass of aircraft NO_x emissions leads to substantially

371 different, sometimes unrealistic, relative increases of aircraft NO_x (Table 1), which means that
372 each regional domain is pushed to different regimes of its local $\text{NO}_x\text{-O}_3\text{-CH}_4$ system, when it
373 'deals' with additional NO_x . In order to try to preserve the subtle balance of regional $\text{NO}_x\text{-O}_3\text{-}$
374 CH_4 systems with the existing emission patterns of aircraft and background NO_x , the
375 experiments with equal relative aircraft NO_x emissions are employed (Table 1).

376
377 The net NO_x radiative forcing from regional perturbations are found to be greater for
378 experiments with lower aircraft NO_x emission rates, which is the 5% (N) yr^{-1} case and tend to
379 decrease with greater aircraft NO_x emissions (Table 4). The net NO_x RFs of EUR, NA and
380 NATL are larger by ~33% for 5% (N) yr^{-1} compared with 0.035 Tg(N) yr^{-1} , the difference for
381 NPAC's net NO_x RF increases to 157%. The short-term O_3 RF variation ranges from 10% for
382 NA to 44% for NPAC; CH_4 RF variation ranges from up to 8% for continental regions and
383 rises significantly for oceanic regions reaching 64% for NATL. In general, for smaller aircraft
384 NO_x emissions rates short-term O_3 RF is calculated to be the greatest and CH_4 RF, and
385 consequently CH_4 -induced O_3 RF and SWV RF are calculated to be the smallest (less
386 negative) compared with greater aircraft NO_x emissions rates.

387
388 There is one exception, SE ASIA: the values of net NO_x RFs for different incremental aircraft
389 NO_x emission cases stay within a ~2% range. The SE ASIA short-term O_3 RF increases with
390 increasing NO_x emission rates and it is observed to be 7% lower for 5% (N) yr^{-1} compared
391 with 0.035 Tg(N) yr^{-1} , and 1% different for 100% (N) yr^{-1} compared with 0.035 Tg(N) yr^{-1} .

392
393 The background atmospheric conditions of SE ASIA domain might explain this distinct
394 behaviour. The HO_x background at flight level over SE ASIA is one of the highest, next to
395 BR, among all investigated regions (Figure 6), having at the same time low NO_x background
396 (< 1 pbbv). Under this condition an important termination chain for HO_2 would be $\text{HO}_2 + \text{HO}_2$
397 (Seinfeld and Pandis, 2006). This finds further explanations in Lin et al. (1988) box model
398 study, where it is shown that for low NO_x background the radical combination reactions (RO_2
399 and HO_2) suppress the non-linearity of O_3 production efficiency. Additionally, Wu et al. (2009)
400 found that the non-linearity of O_3 production, but in the continental boundary layer, is much
401 weaker for NO_x -limited conditions.

402
403 It is worth to note that SE ASIA is much larger than other investigated geographical regions;
404 thus, e.g., it represents a wider range of meteorological phenomena over the year. However, as

405 it is presented in Supplementary Information (SI), it is not likely that the size of the domain
406 might influence the observed linearity of SE ASIA's effects.

407
408 The regional ratios of the CH₄ lifetime change per O₃ burden change vary with different sizes
409 of emitted aircraft NO_x and they decrease with increasing aircraft NO_x emissions (Figure 9).
410 The greatest differences are found to be over oceans, where the CH₄ lifetime change per O₃
411 burden change varies by 54% for NATL and 47% for NPAC between aircraft emissions of
412 0.71 and 1.42 Tg(N) yr⁻¹; the continental (EUR and NA) differences constitute ~10% between
413 0.71 and 1.8 Tg(N) yr⁻¹. The CH₄ lifetime change per O₃ burden change for SE ASIA varies
414 only by 3% for different aircraft NO_x emissions rates, which results in relatively constant
415 magnitudes of net NO_x RFs (Table 4). The regional metric values are significantly correlated
416 with ratio of CH₄ lifetime change per O₃ change ($r=0.7$, $p<0.001$). The remote oceanic
417 regions, with small CH₄ lifetime change per O₃ burden change values, give larger net NO_x
418 GWPs than continental regions with greater CH₄/O₃ ratios. In general, regional aviation net
419 NO_x GWPs decrease with increasing aircraft NO_x emissions; consequently, the SE ASIA is
420 again an exception.

421
422 The spread in the reported regional net NO_x RFs and GWPs differs between different
423 experimental designs (Figure 10). Experiments with 0.035 Tg(N) yr⁻¹ have shown reduced
424 variability of calculated metrics, mainly through suppressed NPAC response. The aviation net
425 NO_x GWP varies from 25 (EUR) to 110 (NATL) for 0.035 Tg(N) yr⁻¹ incremental aircraft
426 NO_x emissions experiments. The 5% (N) yr⁻¹ incremental aircraft NO_x emissions case results
427 in new values ranging from 31 for EUR to 256 for NPAC. Regional application of an equal
428 mass and a relative mass of aircraft NO_x emission result in significant difference in the
429 magnitudes of calculated metrics that constitutes ~49%, as an average among investigated
430 regions.

431

432

433

434

435

436

437

438

439 **6 Conclusions**

440
441 Aircraft NO_x emissions injected into different geographical locations, based on MOZART-3
442 simulations, affect the sensitivities of global chemical responses and the compensating
443 balance between O₃ and CH₄ is specific for each regional domain. The resultant O₃ burden
444 change varies by 54% between different regions, where Europe and Australia result in lowest
445 and greatest O₃ perturbation, respectively. The aviation net NO_x GWP₁₀₀ varied from 25 for
446 Europe to 110 for the North Atlantic (based on 0.035 Tg(N) yr⁻¹ incremental aircraft NO_x
447 emission experiments). Significant hemispherical disparity in the resultant effects from
448 aircraft NO_x perturbation was also found, where Southern Hemisphere's short-term and long-
449 term responses were twice greater than those for Northern Hemisphere. The remote oceanic
450 region of North Atlantic, along with tropical Brazil, turned out to result in the greatest
451 magnitude of aircraft net NO_x effect, ~10.0 mW m⁻²/Tg(N) yr⁻¹. The low-latitudinal regions
452 appeared also to have the greatest compensation between the short-term O₃ effect and long-
453 term CH₄ responses that efficiently reduced their net NO_x climate impacts.

454
455 The regional chemical perturbations varies with the size of aircraft NO_x emission rate;
456 therefore, experiments based on equal mass of aircraft NO_x emissions might imply violation
457 of the subtle balance of the regional NO_x-O₃-CH₄ systems. This affects mainly geographical
458 domains with low NO_x concentration (e.g., remote oceanic regions), where injected NO_x often
459 constitutes a significant relative increase, which pushes the local NO_x-O₃-CH₄ balance into a
460 saturation regime and reduces its aircraft NO_x effect. The experiments with small equal
461 relative aircraft NO_x emissions revealed the new potential of regional aircraft NO_x effects. The
462 greatest effect was observed for North Pacific with its net NO_x RF of 23.7 mW m⁻²/Tg(N)yr⁻¹.
463 The 5% (N) yr⁻¹ incremental aircraft NO_x emission case resulted in a net aviation NO_x GWP₁₀₀
464 ranging from 31 for Europe to 256 for North Pacific, representing much greater spread in the
465 reported regional metric values.

466
467 The size of the aircraft NO_x emission rate and consequently an experimental approach
468 strongly influence both the magnitudes and the perception of regional dependencies, where
469 e.g., the greatest net NO_x effect interchangeably belongs to either North Pacific or North
470 Atlantic and Brazil. Thus, it is important to apply an appropriate experimental design
471 depending on the nature of investigations.

472

473 **Acknowledgements:** Ivar Isaksen is acknowledged for helpful discussions and anonymous reviewers
474 are thanked for their comments. This work was funded by the United Kingdom Department for
475 Transport.

476
477
478
479

References

480 ACI, 2011. ACI Global Traffic Forecast 2010-2029. Airports Council International, Montreal, Canada.
481 <http://www.aci.aero/publications>.

482
483 Berntsen T. K., Isaksen I.S.A., 1999. Effects of lightning and convection on changes in tropospheric
484 ozone due to NO_x emissions from aircraft. *Tellus* 51B, 766-788.

485
486 Berntsen, T. K., Fuglestedt J. S., Joshi M. M., Shine K. P., Stuber N., Ponater M., Sausen R.,
487 Hauglustaine D. A., Li L., 2005. Response of climate to regional emissions of ozone precursors:
488 sensitivities and warming potentials. *Tellus, Series B: Chemical and Physical Meteorology* 57, 283-
489 304.

490
491 Brasseur G. P., Hauglustaine D. A., Walters S., Rasch P. J., Müller J.-F., Granier C., Tie X. X., 1998.
492 MOZART, a global chemical transport model for ozone and related tracers, Part 1: Model description.
493 *Journal of Geophysical Research* 103 (21), 28265-28289.

494
495 Collins W. J., Fry M. M., Yu H., Fuglestedt J. S., Shindell D. T., West J. J., 2013. Global and
496 regional temperature change potentials for near-term climate forcers. *Atmospheric Chemistry and*
497 *Physics* 13, 2471-2485.

498
499 Dee D. P., Uppala S. M., Simmons A. J., Berrisford P., Poli P., Kobayashi S., Andrae U., Balmaseda
500 M. A., Balsamo G., Bauer P., Bechtold P., Beljaars A. C. M., van de Berg L., Bidlot J., Bormann N.,
501 Delsol C., Dragani R., Fuentes M., Geer A. J., Haimberger L., Healy S. B., Hersbach H., Hólm E. V.,
502 Isaksen L., Kållberg P., Köhler M., Matricardi M., McNally A. P., Monge-Sanz B. M., Morcrette J. J.,
503 Park B. K., Peubey C., de Rosnay P., Tavolato C., Thépaut J. N., Vitart F., 2011. The ERA-interim
504 reanalysis: configuration and performance of the data assimilation system. *Quarterly Journal of the*
505 *Royal Meteorological Society* 137, 553-597.

506
507 Edwards J. M., Slingo A., 1996. Studies with a flexible new radiation code. I: Choosing a
508 configuration for a large-scale model. *Quarterly Journal of the Royal Meteorological Society* 122, 689-
509 719.

510
511 Fry M. M., Schwarzkopf M. D., Adelman Z., Naik V., Collins W. J., West J. J., 2013. Net radiative
512 forcing and air quality responses to regional CO emission reductions. *Atmospheric Chemistry and*
513 *Physics* 13, 5381-5399.

514
515 Fuglestedt J. S., Berntsen T. K., Isaksen I. S. A., Mao H., Liang X. Z. and Wang W. C., 1999.
516 Climatic forcing of nitrogen oxides through changes in tropospheric ozone and methane; global 3D
517 model studies. *Atmospheric Environment* 33, 961-77.

518

- 519 Fuglestad J. S., Shine K. P., Cook J., Bernsten T., Lee D. S., Stenke A., Skeie R. B., Velders G. J.
520 M., Waitz I. A., 2010. Transport impacts on atmosphere and climate: Metrics. *Atmospheric*
521 *Environment* 44, 4648-4677.
- 522
523 Granier C., Guenther A., Lamarque J. F., Mieville A., Muller J. F., Olivier J., Orlando J., Peters G.,
524 Petron G., Tyndall G., Wallens S., 2005. POET, a database of surface emissions of ozone precursors.
525 (available at <http://www.aero.jussieu.fr/projet/ACCENT/POET.php>).
526
- 527 Grewe V., Stenke A., 2008. Airclim: an efficient tool for climate evaluation of aircraft technology.
528 *Atmospheric Chemistry and Physics* 8, 4621-4639.
- 529
530 Hack J. J., 1994. Parameterization of moist convection in the NCAR community climate model
531 (CCM2). *Journal of Geophysical Research* 99, 5551-5568.
- 532
533 Holstag A., Boville B. A., 1993. Local versus nonlocal boundary-layer diffusion in a global climate
534 model. *Journal of Climate* 6, 1825-1842.
- 535
536 Isaksen I. S. A., Hov Ø., Hesstvedt E., 1978. Ozone generation over rural areas. *Environmental*
537 *Science and Technology* 12, 1279-1284.
- 538
539 Jaeglé L., Jacob D. J., Brune W. H., Tan D., Faloon I. C., Weinheimer A. J., Ridley B. A., Campos T.
540 L., Sachse G. W., 1998. Sources of HO_x and production of ozone in the upper troposphere over the
541 United States. *Geophysical Research Letters* 25, 1709-1712.
- 542
543 Joos F., Roth R., Fuglestad J. S., Peters G. P., Enting I. G., von Bloh W., Brovkin V., Burke E. J.,
544 Eby M., Edwards N. R., Friedrich T., Frölicher T. L., Halloran P. R., Holden P. B., Jones C., Kleinen
545 T., Mackenzie F. T., Matsumoto K., Meinshausen M., Plattner G.-K., Reisinger A., Segschneider J.,
546 Shaffer G., Steinacher M., Strassmann K., Tanaka K., Timmermann A., Weaver A. J., 2013. Carbon
547 dioxide and climate impulse response functions for the computation of greenhouse gas metrics: a
548 multi-model analysis. *Atmospheric Chemistry and Physics* 13, 2793-2825.
- 549
550 Kinnison D. E., Brausser G. P., Walters S., Garcia R. R., Marsh D. R., Sassi F., Harvey V. L., Randall
551 C. E., Emmons L., Lamarque J. F., Hess P., Orlando J. J., Tie X. X., Randel W.,
552 Pan L. L., Gettelman A., Granier C., Diehl T., Niemeier U., Simmons A. J., 2007. Sensitivity of
553 chemical tracers to meteorological parameters in the MOZART-3 chemical transport model, *Journal of*
554 *Geophysical Research* 112, D20302.
- 555
556 Köhler M. O., Rädcl G., Dessens O., Shine K. P., Rogers H. L., Wild O., Pyle J. A., 2008. Impact of
557 perturbations of nitrogen oxide emissions from global aviation. *Journal of Geophysical Research* 113,
558 D11305.
- 559
560 Köhler M. O., Rädcl G., Shine K. P., Rogers H. L., Pyle J. A., 2013. Latitudinal variation of the effect
561 of aviation NO_x emissions on atmospheric ozone and methane and related climate metrics.
562 *Atmospheric Environment* 64, 1-9.
- 563
564 Lamarque J. F., Bond T. C., Eyring V., Granier C., Heil A., Klimont Z., Lee D., Liousse C., Mieville
565 A., Owen B., Schultz M. G., Shindell D., Smith S. J., Stehfest E., Van Aardenne J., Cooper O. R.,
566 Kainuma M., Mahowald N., McConnell J. R., Naik V., Riahi K., van Vuuren D. P., 2010. Historical

- 567 (1850–2000) gridded anthropogenic and biomass burning emissions of reactive gases and aerosols:
568 methodology and application. *Atmospheric Chemistry and Physics* 10, 7017-7039.
- 569
- 570 Lee D. S., Pitari G., Grewe, V., Gierens K., Penner J. E., Petzold A., Prather M., Schumann U., Bais
571 A., Berntsen T., Iachetti D., Lim L. L., Sausen R., 2010. Transport impacts on atmosphere and climate:
572 Aviation. *Atmospheric Environment* 44, 4678-4734.
- 573
- 574 Lin S. J., Rood R. B., 1996. A fast flux form semi-Lagrangian transport scheme on the sphere.
575 *Monthly Weather Review* 124, 2046-2070.
- 576
- 577 Lin X., Trainer M., Liu S. C., 1988. On the nonlinearity of the tropospheric ozone production. *Journal*
578 *of Geophysical Research* 93, 15879-15888.
- 579
- 580 Liu Y., Liu C. X., Wang H. P., Tie X. X., Gao S. T., Kinnison D., Brasseur G., 2009. Atmospheric
581 tracers during the 2003–2004 stratospheric warming event and impact of ozone intrusions in the
582 troposphere. *Atmospheric Chemistry and Physics* 9, 2157-2170.
- 583
- 584 Lund M., Berntsen T., Fuglestedt J., Ponater M., Shine K., 2012. How much information is lost by
585 using global mean climate metrics? an example using the transport sector. *Climatic Change*, 113, 949-
586 963.
- 587
- 588 Müller J.-F., 1992. Geographical distribution and seasonal variation of surface emissions and
589 deposition velocities of atmospheric trace gases. *Journal of Geophysical Research* 97, 3787-3804.
- 590
- 591 Myhre G., Highwood E. J., Shine K. P., Stordal F., 1998, New estimates of radiative forcing due to
592 well mixed greenhouse gases. *Geophysical Research Letters* 25, 2715-2718.
- 593
- 594 Myhre G., Nilssen J.S., Gulstad L., Shine K.P., Rognerud B., Isaksen I. S. A., 2007. Radiative forcing
595 due to stratospheric water vapour from CH₄ oxidation. *Geophysical Research Letters* 34, L01807.
- 596
- 597 Myhre G., Shine K. P., Rädcl G., Gauss M., Isaksen I. S. A., Tang Q., Prather M. J., Williams J. E.,
598 van Velthoven P., Dessens O., Koffi B., Szopa S., Hoor P., Grewe V., Borken-Kleefeld J., Berntsen T.
599 K., Fuglestedt J. S., 2011. Radiative forcing due to changes in ozone and methane caused by the
600 transport sector. *Atmospheric Environment* 45, 387-394.
- 601
- 602 Myhre G., Shindell D., Bréon F.-M., Collins W., Fuglestedt J., Huang J., Koch D., Lamarque J.-F.,
603 Lee D., Mendoza B., Nakajima T., Robock A., Stephens G., Takemura T., Zhang H., 2013.
604 Anthropogenic and natural radiative forcing. *Climate Change 2013: the Physical Science Basis.*
605 Contribution of Working Group I to the Fifth Assessment Report of the Intergovernmental Panel on
606 Climate Change. Cambridge University Press, Cambridge, United Kingdom and New York, NY, USA.
- 607
- 608 Prather M., Sausen R., Grossmann A. S., Haywood J. M., Rind D., Subbaraya B. H., 1999. Potential
609 climate change from aviation. Chapter 6 of 'Aviation and the global atmosphere'. In: Penner J. E., et
610 al. (Eds.), *Special Report of the Intergovernmental Panel on Climate Change*. Cambridge University
611 Press, Cambridge.
- 612
- 613 Rossow W. B., Schiffer R. A., 1999. Advances in understanding clouds from ISCCP, *Bulletin of*
614 *the American Meteorological Society* 80, 2261-2288.

- 615
616 Sander S., Friedl R., Ravishankara A., Golden D., Kolb C., Kurylo M., Molina M.,
617 Moortgat G., Finlayson-Pitts B., Wine P., Huie R., Orkin V., 2006. Chemical kinetics and
618 photochemical data for use in atmospheric studies – evaluation number 15. Technical report, Jet
619 Propulsion Laboratory (JPL) of the National Aeronautics and Space Administration (NASA).
620
- 621 Sassi F., Kinnison D. E., Boville B. A., Garcia R. R., Roble R., 2004. Effect of El Niño – Southern
622 Oscillation on the dynamical, thermal, and chemical structure of the middle atmosphere. *Journal of*
623 *Geophysical Research* 109, D17108.
624
- 625 Shindell D. T., 2012. Evaluation of the absolute regional temperature potential. *Atmospheric*
626 *Chemistry and Physics* 12, 7955-7960.
627
- 628 Shine K., Berntsen T., Fuglestedt J., Sausen R., 2005. Scientific issues in the design of metrics for
629 inclusion of oxides of nitrogen in global climate agreements. *Proceedings of the National Academy of*
630 *Sciences of the United States of America* 102, 44, 15768-15773.
631
- 632 Skowron A., Lee D. S., De Leon R. R., 2013. The assessment of the impact of aviation NO_x on ozone
633 and other radiative forcing responses – The importance of representing cruise altitudes accurately.
634 *Atmospheric Environment* 74, 159-168.
635
- 636 Søvde O. A., Matthes S., Skowron A., Iachetti D., Lim L., Owen B., Hodnebrog Ø., Di Genova G.,
637 Pitari G., Lee D. S., Myhre G., Isaksen I. S. A., 2014. Aircraft emission mitigation by changing route
638 altitude: A multi-model estimate of aircraft NO_x emission impact on O₃ photochemistry. *Atmospheric*
639 *Environment* 95, 468-479.
640
- 641 Stevenson D. S., Doherty R. M., Sanderson M. G., Collins W. J., Johnson C. E., Derwent R.G., 2004.
642 Radiative forcing from aircraft NO_x emissions: Mechanisms and seasonal dependence. *Journal of*
643 *Geophysical Research* 109, D17307.
644
- 645 Stevenson D. S., Derwent R. G., 2009. Does the location of aircraft nitrogen oxide emissions affect
646 their climate impact? *Geophysical Research Letters* 36, L17810.
647
- 648 Wu S. L., Duncan B. N., Jacob D. J., Fiore A. M., Wild O., 2009. Chemical nonlinearities in relating
649 intercontinental ozone pollution to anthropogenic emissions. *Geophysical Research Letters* 36,
650 L05806.
651
- 652 Wuebbles D. J., Patten K. O., Wang D., Youn D., Martínez-Avilés M., Francisco J. S., 2011. Three-
653 dimensional model evaluation of the Ozone Depletion Potentials for n-propyl bromide,
654 trichloroethylene and perchloroethylene. *Atmospheric Chemistry and Physics* 11, 2371-2380.
655
- 656 Zhang G. J., McFarlane N. A., 1995. Sensitivity of climate simulations to the parameterization of
657 cumulus convection in the Canadian climate centre general circulation model.
658 *Atmosphere-Ocean* 33, 407-446.

Table SI 1: Normalized aircraft net NO_x radiative forcings for different Asian incremental aircraft NO_x emissions. Net NO_x accounts for short-term O₃ RF, CH₄-induced O₃ RF and CH₄ with SWV RF

REGION	Net NO _x RF [mW m ⁻² /Tg(N) yr ⁻¹]		
	0.035 Tg(N) yr ⁻¹	5 % (N) yr ⁻¹	100 % (N) yr ⁻¹
SE ASIA	5.33	5.26	5.25
S ASIA	6.51	6.67	6.35
E ASIA	4.65	4.59	4.46

Table 1: Description of regional domains along with changes in aircraft NO_x emissions for a series of experimental cases and each regional domain.

REGION	Geographical extent	Aircraft NO _x [Tg(N) yr ⁻¹]	Fixed mass incremental aircraft N			Relative incremental aircraft N*	
			[Δ N/base N]			[Tg(N) yr ⁻¹]	
			0.035 Tg(N) yr ⁻¹	0.71 Tg(N) yr ⁻¹	6.39 Tg(N) yr ⁻¹	5% (N) yr ⁻¹	100% (N) yr ⁻¹
EUR	10°W-30°E; 40°N-60°N	0.112	0.32	6.3	57.2	0.006	0.112
NA	120°W-75°W; 30°N-50°N	0.132	0.27	5.4	48.5	0.007	0.132
SE ASIA	95°E-145°E; 12°S-45°N	0.128	0.28	5.5	50.0	0.006	0.128
NPAC	180°W-140°W; 150°E-180°E; 20°N-60°N	0.021	1.67	33.4	300.6	0.001	0.021
NATL	50°W-15°W; 30°N-60°N	0.023	1.54	30.8	276.8	0.001	0.023
BR	60°W-36°W; 36°S-6°S	0.010	4.43	69.7	–	–	–
SAFR	16°E-32°E; 36°S-18°S	0.003	12.2	224.2	–	–	–
AU	134°E-154°E; 38°S-22°S	0.009	4.84	78.0	–	–	–
NH	180°W-180°E; 0°-90°N	0.653	0.05	1.1	9.8	0.033	0.653
SH	180°W-180°E; 0°-90°S	0.057	0.62	12.4	111.9	0.003	0.057
Global	180°W-180°E; 90°S-90°N	0.71	0.05	1	9	0.035	0.71

*The regions BR, SAFR and AU were excluded from these experiments, as aircraft NO_x emissions for these regions are marginal, their contribution to aircraft NO_x global total constitute 1.5%, 0.5% and 1.3%, respectively. Thus, the signal from any small relative incremental aircraft NO_x emissions experiments for these regions is barely visible in CTM results.

Table 2: The global and annual mean O₃ burden change (in Tg) and the CH₄ lifetime reduction (in yr) due to the aircraft NO_x emissions in different geographical regions. Calculations are done for surface–1hPa domain and are based on 0.035 Tg(N) yr⁻¹ incremental aircraft NO_x emission. All values are on a per Tg N basis. The CH₄ lifetime for the year 2006, as modelled by MOZART-3, is 8.5 years.

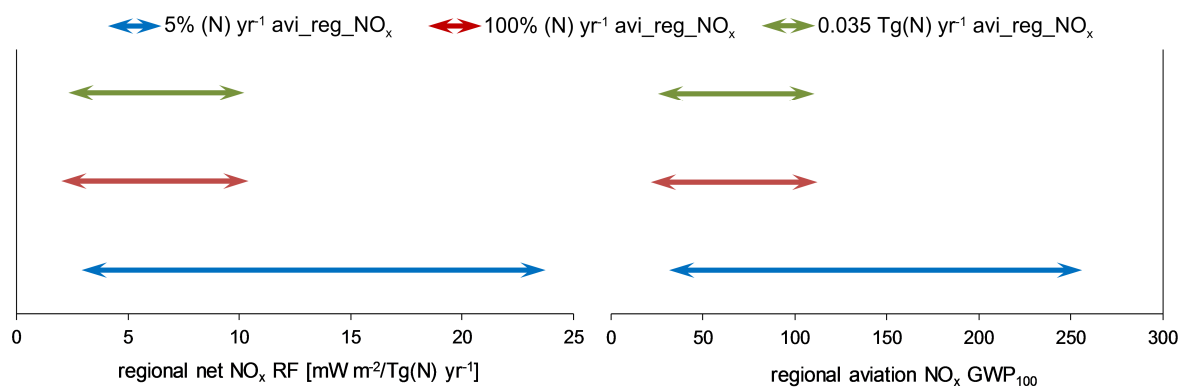
REGION	O ₃ burden change	CH ₄ lifetime change
	(Tg)	(yr)
Global	5.65	-0.081
NH	5.33	-0.074
SH	8.82	-0.160
EUR	4.22	-0.057
NA	4.73	-0.067
SE ASIA	5.51	-0.093
NPAC	7.28	-0.087
NATL	6.32	-0.057
BR	7.94	-0.158
SAFR	7.77	-0.139
AU	9.11	-0.173

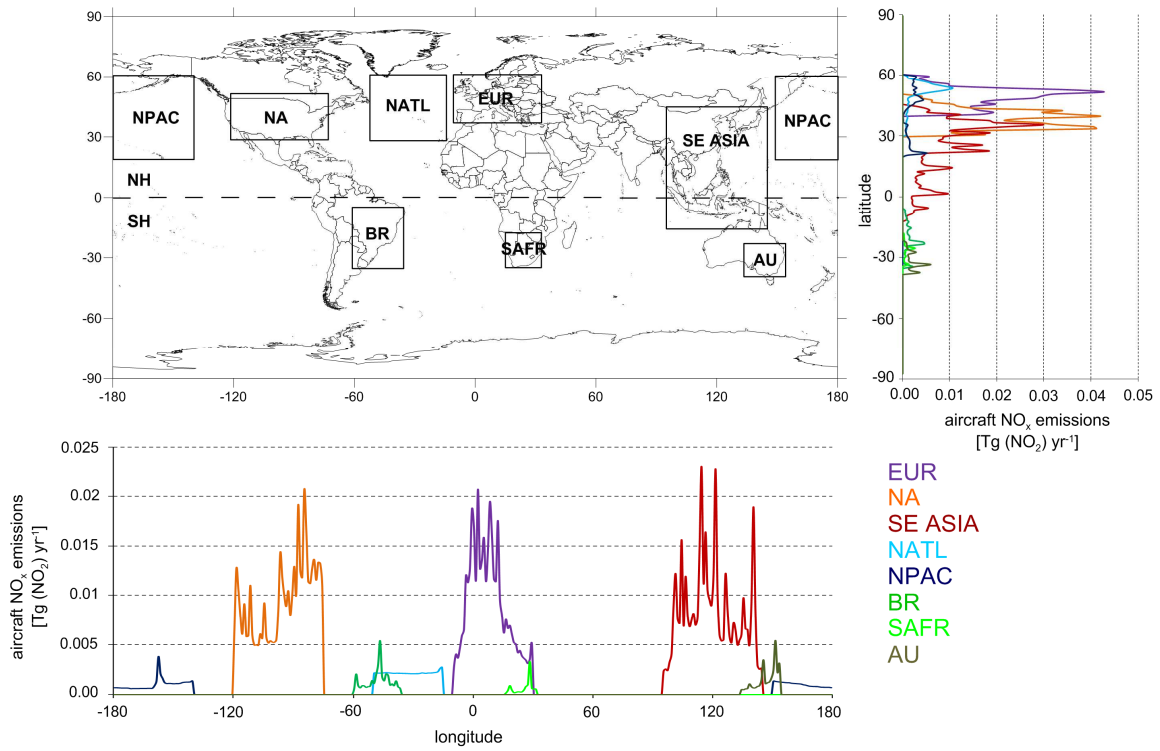
Table 3: Aviation net NO_x Global Warming Potentials (GWP) for Northern and Southern Hemisphere and regions: Europe, North America, Southeast Asia, North Atlantic, North Pacific, Brazil, South Africa and Australia for 20-, 100- and 500-year time horizons. All values are on a per kg N basis relative to CO₂ and are based on 0.035 Tg(N) yr⁻¹ incremental aircraft NO_x emissions.

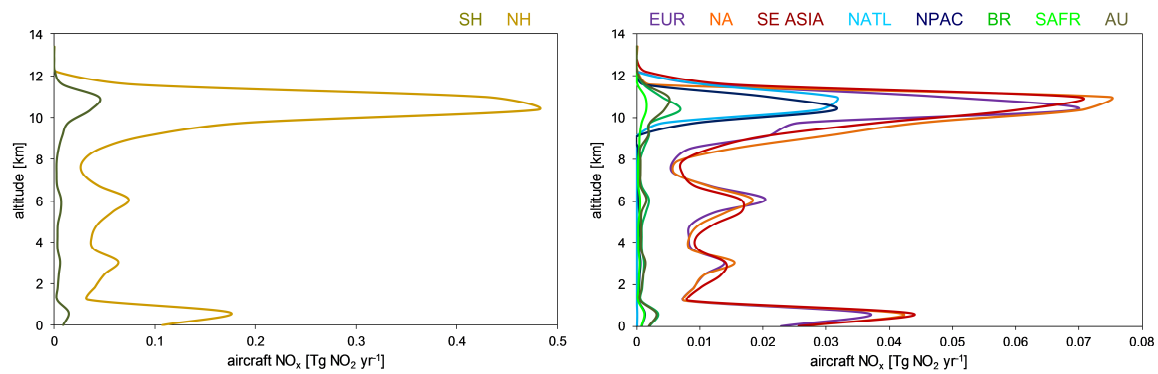
REGION	GWP		
	H=20	H=100	H=500
Global	322	59	17
NH	305	57	16
SH	458	70	20
EUR	164	25	7
NA	234	40	11
SE ASIA	329	57	16
NPAC	477	99	28
NATL	478	110	31
BR	542	109	31
SAFR	416	70	20
AU	480	87	25

Table 4: Normalized aircraft net NO_x radiative forcings for different regional incremental aircraft NO_x emissions. Net NO_x accounts for short-term O₃ RF, CH₄-induced O₃ RF and CH₄ with SWV RF.

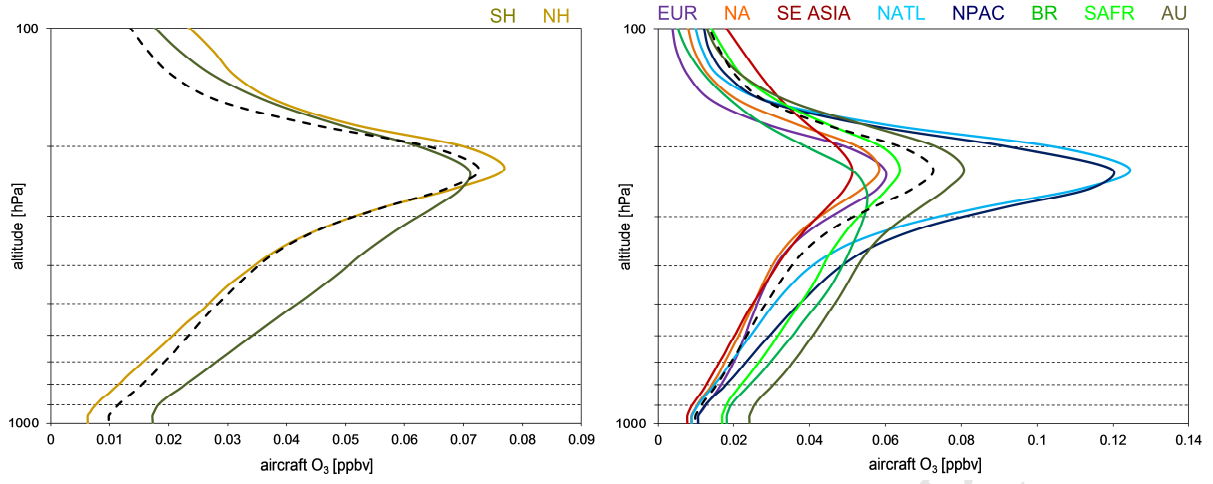
REGION	Net NO _x RF [mW m ⁻² /Tg(N) yr ⁻¹]		
	0.035 Tg(N) yr ⁻¹	5 %(N) yr ⁻¹	100 %(N) yr ⁻¹
Global	5.51	5.51	4.89
NH	5.31	5.32	4.76
SH	6.45	9.02	6.42
EUR	2.32	2.90	1.97
NA	3.73	5.07	3.52
SE ASIA	5.33	5.26	5.25
NPAC	9.22	23.73	9.53
NATL	10.21	14.06	10.38

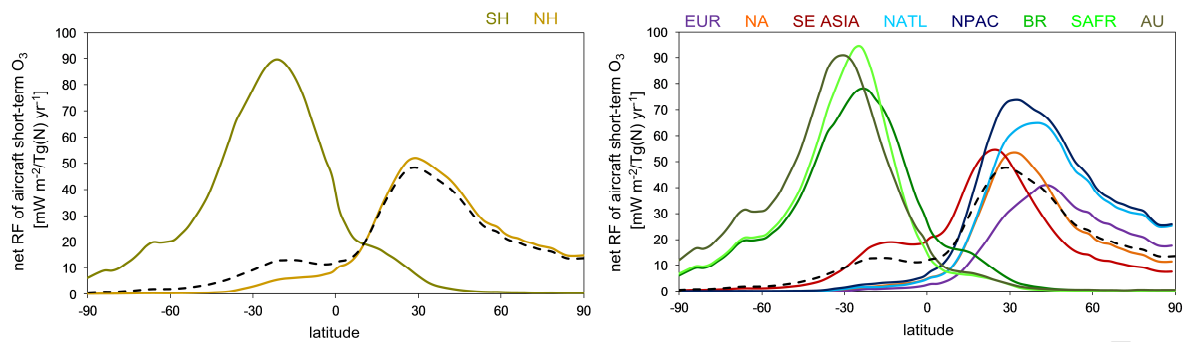


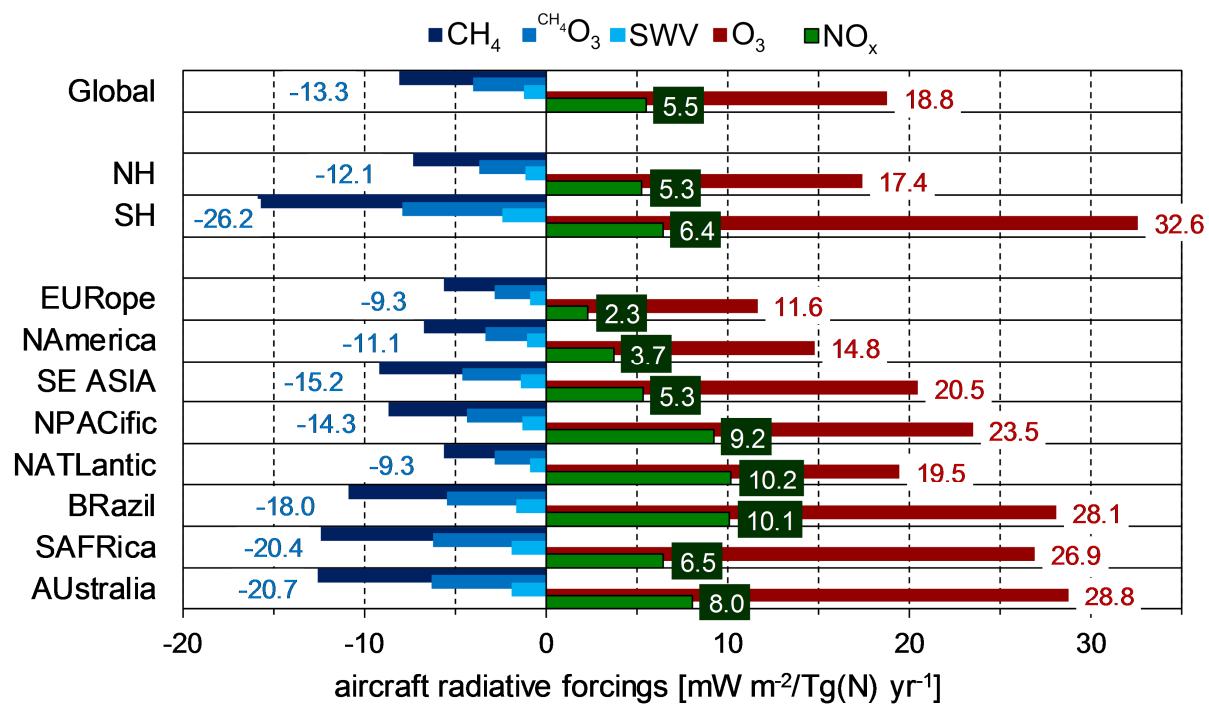


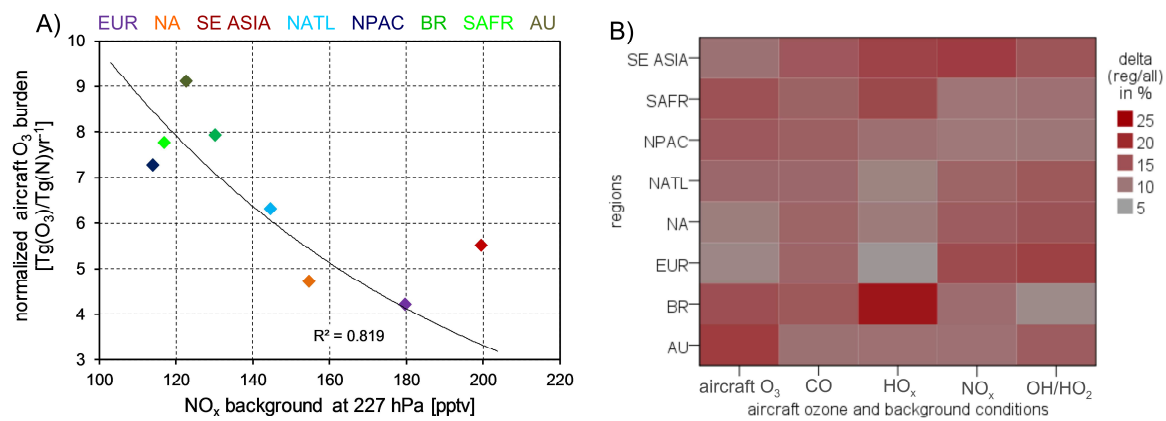


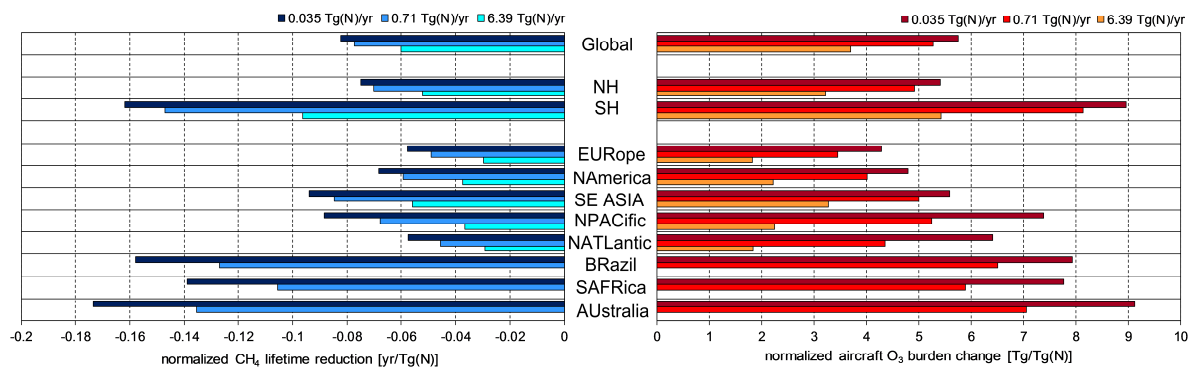
ACCEPTED MANUSCRIPT

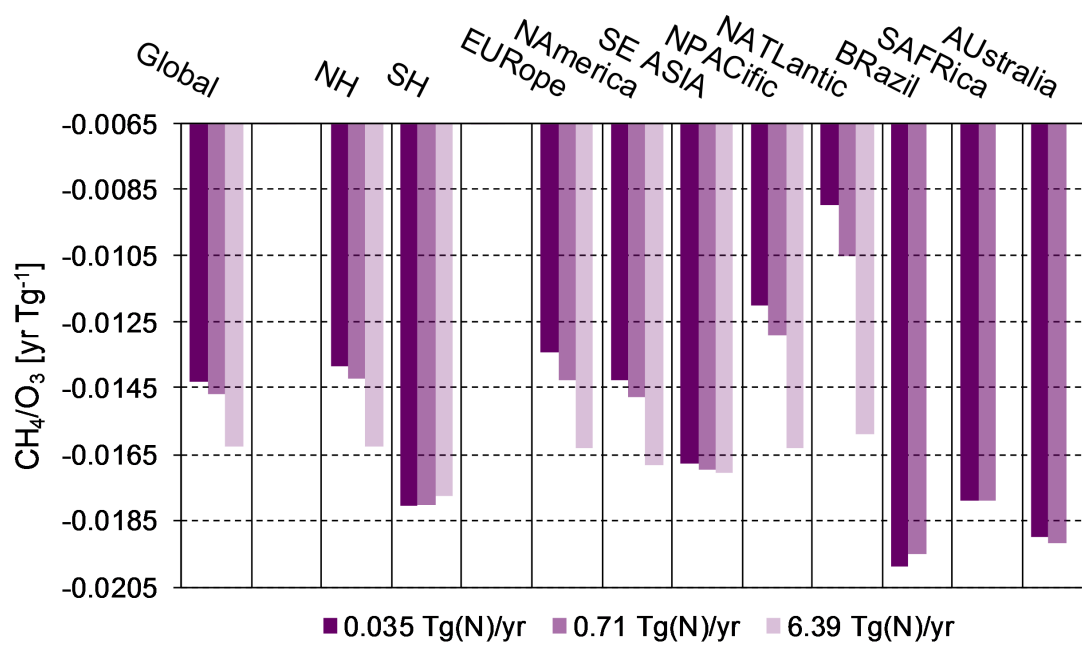


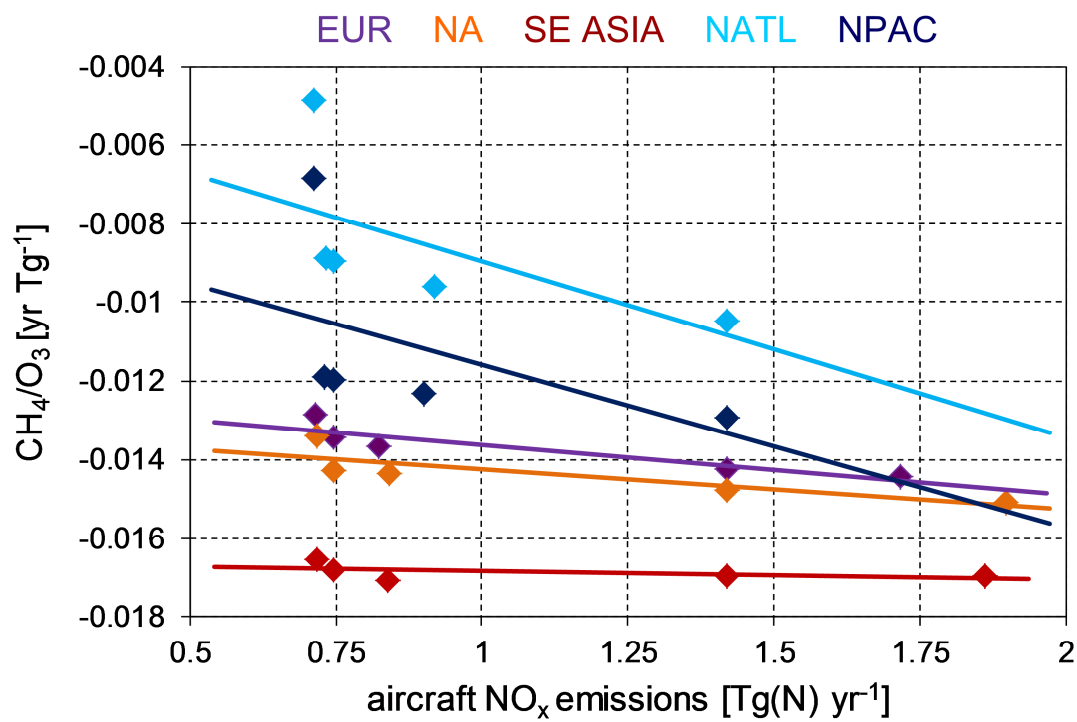














ACCEPTED MANUSCRIPT

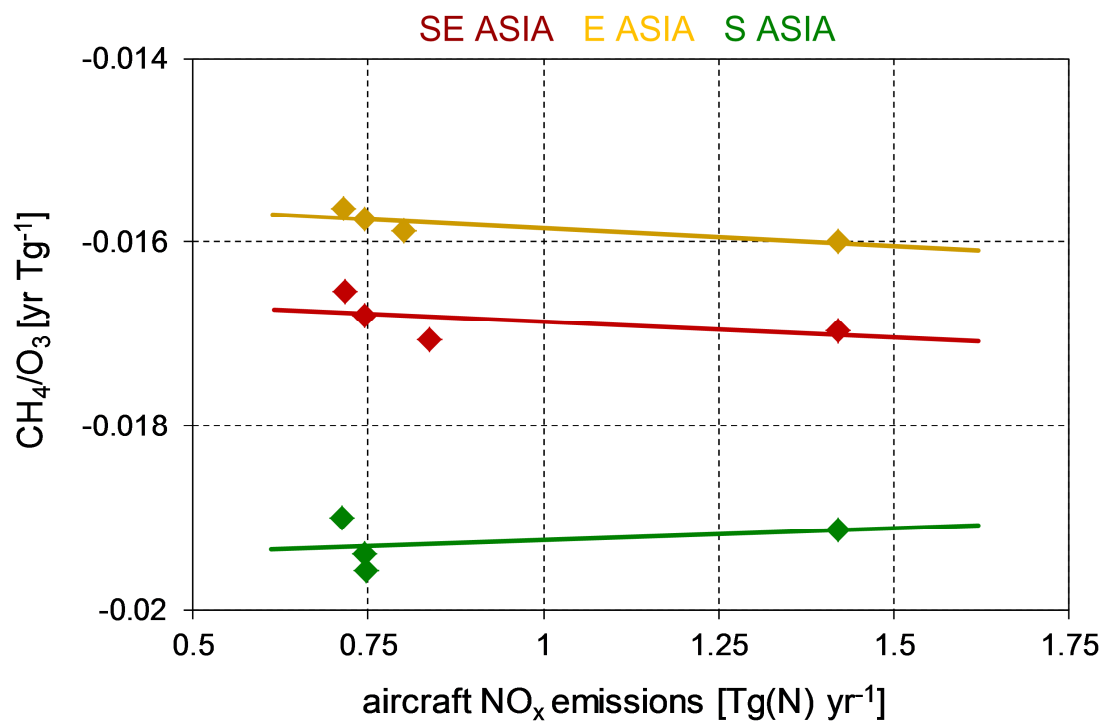


Figure SI 1: SE ASIA domain partitioned to smaller domains: E ASIA and S ASIA.

Figure SI 2: Scatter plot of CH₄ lifetime change per O₃ burden change for different Asian domains and a series of aircraft NO_x emission (dots are individual experiments, lines are the linear best fit lines).

ACCEPTED MANUSCRIPT

Figure 1: Regional domains selected for this study: Europe (EUR), North America (NA), Southeast Asia (SE ASIA), North Atlantic (NATL), North Pacific (NPAC), Brazil (BR), South Africa (SAFR), Australia (AU), Northern Hemisphere (NH) and Southern Hemisphere (SH), along with latitudinal (right panel) and longitudinal (bottom panel) profiles of regional aircraft NO_x emissions.

Figure 2: The vertical profiles of regional aircraft NO_x emissions: Northern and Southern Hemisphere (left panel); Europe (EUR), North America (NA), Southeast Asia (SE ASIA), North Atlantic (NATL), North Pacific (NPAC), Brazil (BR), South Africa (SAFR) and Australia (AU) (right panel).

Figure 3: The global and annual mean vertical distributions of O_3 changes (in ppbv) for aircraft NO_x emission increases by $0.035 \text{ Tg(N) yr}^{-1}$ in different regional domains: Northern (NH) and Southern (SH) Hemispheres (left panel), Europe (EUR), North America (NA), Southeast Asia (SE ASIA), North Atlantic (NATL), North Pacific (NPAC), Brazil (BR), South Africa (SAFR) and Australia (AU) (right panel). The dashed black line represents the O_3 change from global aircraft NO_x emission.

Figure 4: Zonal and annual mean net (long wave and shortwave) radiative forcing ($\text{mW m}^{-2}/\text{Tg(N) yr}^{-1}$) from short-term O_3 for Northern (NH) and Southern (SH) Hemisphere (left panel) and regions: Europe (EUR), North America (NA), Southeast Asia (SE ASIA), North Atlantic (NATL), North Pacific (NPAC), Brazil (BR), South Africa (SAFR) and Australia (AU) (right panel). Based on $0.035 \text{ Tg(N) yr}^{-1}$ incremental aircraft NO_x experiments. The dashed black line represents the O_3 RF from global aircraft NO_x emission.

Figure 5: Radiative forcings per unit emission of N (in $\text{mW m}^{-2}/\text{Tg(N) yr}^{-1}$) due to short-term O_3 (O_3), CH_4 -induced O_3 ($^{\text{CH}_4}\text{O}_3$), CH_4 (CH_4), stratospheric water vapour (SWV) and NO_x (net of all 4 components) for Northern and Southern Hemisphere and regions: Europe, North America, Southeast Asia, North Atlantic, North Pacific, Brazil, South Africa and Australia. The short-term forcing values are given in red, the long-term forcing values (sum of CH_4 , $^{\text{CH}_4}\text{O}_3$ and SWV) are shown in blue and the net NO_x RF magnitudes are presented in green. Based on $0.035 \text{ Tg(N) yr}^{-1}$ incremental aircraft NO_x experiments.

Figure 6: Relationship between background conditions and aircraft O_3 burden change. A) Scatter plot of global and annual O_3 burden change due to aircraft NO_x emission increase by $0.035 \text{ Tg(N) yr}^{-1}$ in different regions against background NO_x concentration at 227 hPa (dots are individual experiments, line is the best-fit curve). B) Heat map of background conditions (CO concentrations, HO_x concentrations, NO_x concentrations and OH/HO_2 ratio) at 227 hPa and aircraft O_3 burden change (aircraft O_3) for different regional domains. All variables are presented as an annual mean. The percentage fraction presents how the specific combination of region and background condition contribute to the specific total regional background condition.

Figure 7: The normalized O_3 burden change (red bars) and CH_4 lifetime reduction (blue bars) for a series of geographical regions and aircraft NO_x emission rates.

Figure 8: The ratio of the CH₄ lifetime change to the O₃ change for a series of geographical regions and aircraft NO_x emission rates.

Figure 9: Scatter plot of CH₄ lifetime change per O₃ burden change for different regions and a series of aircraft NO_x emission (dots are individual experiments, lines are the linear best fit lines).

Figure 10: The spread in regional aviation net NO_x RFs (left) and aviation net NO_x GWPs (right) for different incremental aircraft NO_x emission, 5% (N) yr⁻¹ (blue), 100% (N) yr⁻¹ (red) and 0.035 Tg(N) yr⁻¹ (green).

- The effects from hemispherical/regional aircraft NO_x emissions are explored using 3D CTM, MOZART-3.
- The climate metrics values decrease with increasing regional aircraft NO_x emission rates, except for Southeast Asia.
- Regional applications of an equal mass and a relative mass of aircraft NO_x emission result in different regional dependencies.
- The greatest net NO_x radiative forcing is observed for remote northern oceanic regions.

Supplementary Information:

Variation of radiative forcings and global warming potentials from regional aviation NO_x emissions

Agnieszka Skowron*, David S. Lee and Ruben R. De León

Dalton Research Institute, Manchester Metropolitan University, John Dalton Building, Chester Street, Manchester M1 5GD, United Kingdom.

*Corresponding author. E-mail: a.skowron@mmu.ac.uk, tel: + 44 (0) 161 247 6703 (A. Skowron).

SI 1 Additional experiments

The suppressed non-linearity of O₃ production and net NO_x effects is observed for SE ASIA region (Section 5). In order to investigate whether the size of the SE ASIA domain could influence this behaviour, an additional set of experiments was performed using MOZART-3 CTM.

The SE ASIA domain was partitioned to two smaller geographical regions, E ASIA (95°E-145°E; 20°N-45°N) and S ASIA (95°E-145°E; 12°S-20°N) (Figure SI 1). The methodology of applied experiments is consistent with what is described in Section 2 and the size of injected aircraft NO_x rates is the same as it is presented in Table 1.

The magnitudes of ratio of the CH₄ lifetime change per unit O₃ change vary for different Asian domains (Figure SI 2). The magnitudes of S ASIA's ratio is greater by 15% and E ASIA's ratio is smaller by 6%, compared with SE ASIA CH₄/O₃ magnitude (based on 0.035 Tg(N) yr⁻¹). The CH₄ lifetime change per O₃ burden change for E ASIA and S ASIA varies only by 3% for different aircraft NO_x emissions rates, which, similarly as for SE ASIA, results in relatively constant magnitudes of net NO_x RFs.

The values of net NO_x RFs for E ASIA and S ASIA for different incremental aircraft NO_x emission cases stay within a ~5% range, that is slightly larger than SE ASIA's 2% (Table SI 1). However, as well as for SE ASIA, the short-term O₃ RFs for E ASIA and S ASIA increases with increasing NO_x emission rates and they are observed to be ~3% lower for 5%

36 (N) yr⁻¹ compared with 0.035 Tg(N) yr⁻¹, and 1% different for 100% (N) yr⁻¹ compared with
37 0.035 Tg(N) yr⁻¹.

38

39

ACCEPTED MANUSCRIPT